Reliability analysis of infinite slope under intense rainfall considering soil variability

Ji Yuan*, Iason Papaioannou, Chin Man Mok and Daniel Straub

Engineering Risk Analysis Group, Technische Universität München, Munich, Germany

*Corresponding author. Email: ji.yuan@tum.de

Reliability analysis of infinite slope under intense rainfall considering soil variability

Intense rainfall is a major triggering factor of shallow slope failures. The infiltration of water into soil has a significant impact on pore water pressure buildup, which affects surficial slope stability. The subsurface conditions determining this process are inherently variable and uncertain, motivating a probabilistic analysis of slope failure. We investigate the wetting front development in a spatially variable soil and its influence on the reliability of the slope. The vertical variability of permeability parameters and its associated uncertainty are described through random field modeling of saturated hydraulic conductivity and suction head. The discretization of the random fields results in a layered model of the soil. The stability of the slope during the infiltration process is assessed through a time-dependent model that combines the classical infinite slope equation with a one-dimensional infiltration model based on the Green and Ampt assumptions. Subset Simulation is applied to estimate slope reliability. A numerical example is analyzed to demonstrate the influence of vertical soil variability.

Keywords: Intense rainfall; Vertical variability; Time-dependent model; Random field; Subset Simulation

Subject classification codes: 60K10

1. Introduction

Rainfall-induced landslides are a common threat to lives and properties (Polemio 1997, Corominas et al. 2002, Takara and Yamashiki 2011). Intense rainfall events often lead to shallow slope failures (Polemio et al. 2000). The stability of a slope varies with time as rainwater infiltrates into the slope and slope failures occur more frequently in wet seasons. In contrary to conventional slope stability analysis, transient reliability analysis can capture the time-dependent variability of slope stability and uncertainty during the rainfall infiltration process (Yeh et al. 2008, Santoso et al. 2011). The results can provide a basis for near-real-time decision-making and evacuation planning with ample

warning to mitigate losses and to protect human lives.

In many observed cases of shallow slope failure, the failure surfaces are approximately parallel to the ground surface. Soil variability parallel to the groundwater surface is normally less than the vertical variability. Therefore, it is often reasonable to employ an infinite slope model with layering parallel to the ground surface to represent subsurface infiltration as well as the shallow slope failure mechanism (Wu and Abdel-Latif 2000, Muntohar and Liao 2010, Santoso et al. 2011). Since subsurface infiltration is predominately driven by gravitation, the infinite slope is often simplified in practice as a column subject to vertical infiltration, unless topography is very steep.

In this paper, rainfall infiltration is modeled by applying the one-dimensional Green and Ampt simplification (Green and Ampt 1911, Chen and Young 2006), which assumes a distinct border between a "perfectly wetted" (saturated) zone and a "perfectly dry" (in-situ condition prior to rainfall) zone. By further assuming that the potential slip surface is parallel to the ground surface, the infiltration model can be combined with the classical equation for infinite slope stability analysis to evaluate the time-dependent behavior of the factor of safety of the slope. Green and Ampt assumptions are more accurate in highly permeable soils, e.g. dry sandy soils, than in clayey soils where a well defined wetting front is typically not identified (Bauters et al. 2000). Hence, the presented model is mostly applicable to highly permeable soils.

Hydrogeologic parameters are highly heterogeneous, even within a lithological zone that appears to be homogeneous (Phoon and Kulhawy 1999). In this paper, we consider the inherent vertical variability of two hydrogeologic parameters: hydraulic conductivity and suction head. These two parameters are modeled as one-dimensional, stationary, and cross-correlated random fields. Through discretization of the random fields, the soil column is represented by a multilayered system. The infiltration process

in the multi-layered soil is modeled by time discretization, assuming that the flow rate remains constant within the wetted zone at each time step (Chu and Marino 2005, Liu et. al. 2008). The statistics of the wetting front development and the slope factor of safety are computed by Monte Carlo simulation (Rubinstein and Kroese 2008). The probability of slope failure is estimated by Subset Simulation, which is an adaptive sampling method that is especially efficient for estimating small failure probabilities in problems with a large number of random variables (Au and Beck 2001, Papaioannou et al. 2015).

The influence of the variability of hydrogeologic properties on the analysis results is investigated using a numerical example of an infinite slope in sandy soil.

2. Stochastic time-dependent model

2.1 Stability of infinite slope

Consider a slice of an infinite slope with unit width as shown in Figure 1. The infinite slope model assumes that the potential slip surface is parallel to the ground surface. The stability of the slope depends on the shear strength of the soil at the slip surface. Linear Mohr-Coulomb failure criterion is assumed. As a result, the soil shear strength depends on the effective cohesion c' , effective friction analysis φ' , and pore water pressure u at the slip surface. The factor of safety of the slip surface of the slope is given as (e.g. Griffiths et al. 2011):

$$FS = \frac{(\gamma H \cos^2 \beta - u)\tan\varphi' + c'}{\gamma H \sin\beta \cos\beta} \tag{1}$$

in which, γ is the average unit weight of the soil mass above the slip surface; H is the depth of the slip surface in the vertical direction z; β is the slope inclination.

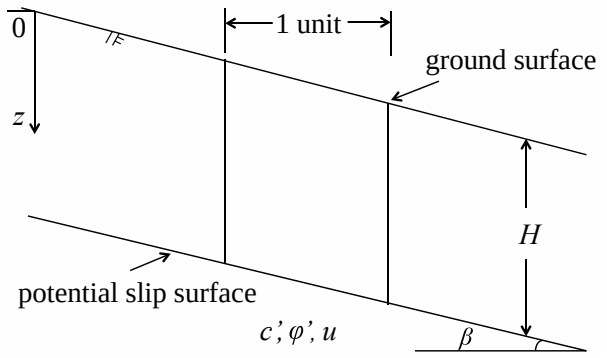

Figure 1. Unit slice in an infinite slope

2.2 Stochastic model of permeability parameters

Griffiths et al. (2011) conduct reliability analysis under specific pore pressure condition to account for the variability of soil strength parameters with depth. In our contribution, the focus is on the pore water pressure, which varies with time and space due to rainwater infiltration. The infiltration process, which affects the pore water pressure u during the wetting front development, is governed by the vertical saturated hydraulic conductivity K and suction head S of the soil. In this study, we account for the vertical variability of these two parameters.

Hydrogeologic parameters are often assumed to follow a lognormal distribution (Gelhar 1986). Consequently, we model the decimal logarithms of the parameters $\log_{10}$K and $\log_{10}$S as homogeneous Gaussian random fields, with the assumption that the autocorrelation coefficient function of the logarithms of both fields is given by the following exponential model (Vanmarcke 1983):

$$\rho(\tau) = e^{-\frac{2\tau}{r}} \tag{2}$$

where r is the scale of fluctuation; τ is the absolute distance between two locations in the vertical direction. The scale of fluctuation is a measure of the spatial variability of the random field. A scale of fluctuation that is much larger than the depth of the soil

slice implies a uniform soil profile; in such case, the saturated hydraulic conductivity and suction head can be modeled by random variables instead of random fields. In the extreme case where the scale of fluctuation is close to zero, the values of the saturated hydraulic conductivity at all locations become independent of each other. Figure 2 shows realizations of a Gaussian random field representing the decimal logarithm of the saturated hydraulic conductivity of a soil column for scales of fluctuation $0.05\mathrm{m}$ and $5\mathrm{m}$. One can observe that the spatial variability is higher as the scale of fluctuation becomes smaller.

The cross-correlation coefficient function, describing the cross-correlation of the logarithms of the two random fields at locations separated by τ is given by:

$$\rho_{cross}(\tau) = \rho_c \cdot \rho(\tau) \tag{3}$$

where ρ_c is the point-wise cross-correlation between the two fields. The saturated hydraulic conductivity and suction head are negatively correlated because the suction tends to increase as the soil becomes less permeable, hence typically $-1 < \rho_c < 0$.

The continuous random fields are discretized by the midpoint method (Der Kiureghian and Ke 1988). The unit slice is divided into a number n of equal-thickness layers; each randomized property is assumed to be constant within each layer, represented by a random variable corresponding to the value of the random field at the midpoint of the layer. Hence the two random fields are represented by a total of $2n$ random variables, gathered in a random vector X. Since homogenous fields are assumed, the means $\mu_{\log_{10}K}$, $\mu_{\log_{10}S}$ and standard deviations $\sigma_{\log_{10}K}$, $\sigma_{\log_{10}S}$ of the random variables corresponding to the discrete layers are constant over the entire field. The entries of the $[2n \times 2n]$ correlation matrix R of the logarithms of the soil properties at each layer are evaluated as follows:

$$\mathbf{R} = [R_{pq}]_{2n\times 2n} = \begin{bmatrix} [\rho(\tau_{pq})]_{n\times n} & [\rho_{cross}(\tau_{pq})]_{n\times n} \\ [\rho_{cross}(\tau_{pq})]_{n\times n} & [\rho(\tau_{pq})]_{n\times n} \end{bmatrix}_{2n\times 2n} \quad (4)$$

where τ_{pq} is the distance between the midpoints of layers p and q. Simulation of the soil parameters is performed by simulating the underlying joint normal random variables of all layers with correlation matrix R, e.g. by the Cholesky decomposition method (Horn and Johnson 1985), and taking the 10-power of the resulting samples. The number of layers n should be chosen such that the variability of the random field, described by the auto- and cross-correlation functions, is adequately represented. Guidelines for common correlation models can be found in (Li and Der Kiureghian 1993).

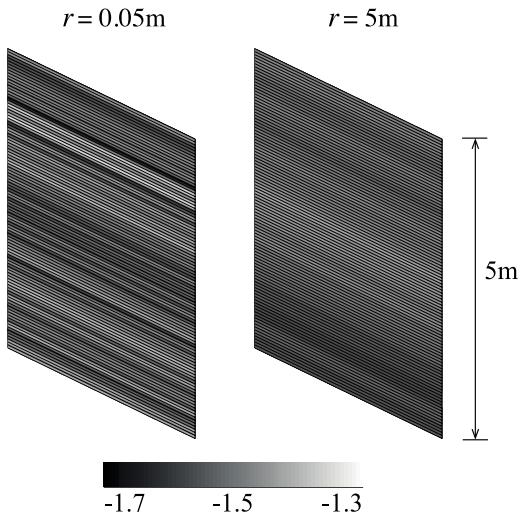

Figure 2. Realizations of $\log_{10}K$ for different scales of fluctuation

2.3 Infiltration analysis

The Green and Ampt assumptions are utilized to simulate the rainwater infiltration process (Green and Ampt 1911). That is, the vertical infiltration of rainwater causes a well-defined wetting front (see Figure 3). Above the wetting front, the soil is fully saturated while below the wetting front it continues to have its initial moisture content. Note that these assumptions are mostly applicable to highly permeable soils, such as

gravel or sandy soils (Chu and Marino 2005).

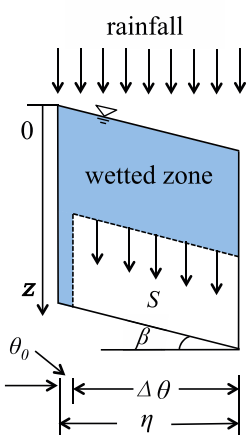

Figure 3. Infiltration process

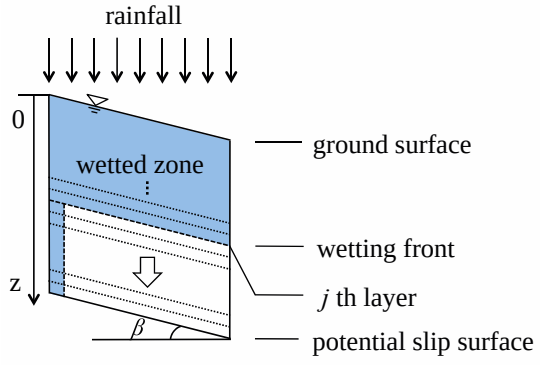

Figure 4. Green and Ampt model on the unit slice

The soil column is divided into a number of equal-thickness layers with varying saturated hydraulic conductivities and suction heads as discussed in Section 2.2. We approach the problem by assuming that the wetting front development takes place in a step-wise manner, whereby the wetting front advances by one layer in each computational step, i.e. in step j the wetting front is exactly located at the bottom of the jth layer (Figure 4). For simplicity, the initial moisture content θ_0 and soil porosity η are considered to be constant within the unit slice (see Figure 3).

This study focuses on intense rainfall events and effective drainage (no ponding above slope surface), during which it is assumed that the rainfall intensity is larger than the infiltration capacity and the pore water pressure at the slope surface is equal to zero. Rainwater infiltrates under gravity. According to Green and Ampt assumptions, the wetting front is pulled down by the suction head (see Figure 3). The hydraulic gradient i from the ground surface to the wetting front at layer j along the vertical direction is obtained by application of Darcy's law:

$$i_j = \frac{z_j + S_j}{z_j} \tag{5}$$

where z_j is the depth of the wetting front at the bottom of the layer j; S_j is the suction head at the wetting front. One can then evaluate the infiltration rate f_j as:

$$f_j = K_{eff,j} \cdot i_j \tag{6}$$

where $K_{eff,j}$ is the effective vertical saturated hydraulic conductivity, corresponding to the harmonic mean of the vertical saturated hydraulic conductivities at the soil layers within the wetted zone (Freeze and Cherry 1979):

$$K_{eff,j} = \frac{j}{\sum_{l=1}^{j} \frac{1}{K_l}} \tag{7}$$

in which K_l is the saturated hydraulic conductivity of the wetted discretization layer l. The cumulative infiltration will be governed by the infiltration capacity and can be obtained as:

$$F_j = z_j \cdot \Delta\theta \tag{8}$$

in which $\Delta\theta$ is the change in moisture content, given as:

$$\Delta\theta = \eta - \theta_0 \tag{9}$$

where η is the porosity of the soil and θ_0 is the initial moisture content (see Figure 3). Noting that $f = dF/dt$, one can obtain the cumulative infiltration time as follows:

$$t_j = \int_0^{t_j} dt = \int_0^{z_j} \frac{\Delta\theta}{f_j} dz \tag{10}$$

Eq. (10) can be evaluated numerically by substituting the integral with a summation over the wetted discretization layers as:

$$t_j = \Delta z \cdot \Delta\theta \cdot \sum_{l=1}^{j} \frac{1}{f_l} \tag{11}$$

where Δz is the thickness of each layer; f_l is the flow rate at the lth wetted discretization layer. Through Eq. (11) one has a direct relationship between time and the wetting front development.

2.4 Pore water pressure distribution

The pore water pressure buildup within the wetted zone varies with time and space, depending on the spatial variability of the saturated hydraulic conductivity and suction head. Due to flow continuity, the effective flow rate of the wetted zone f computed by Eq. (6) equals the flow rate at each wetted layer (Chu and Marino 2005, Liu et. al. 2008), i.e.

$$f_1 = f_2 = \cdots = f_l = \cdots = f_j \tag{12}$$

where f_l is the flow rate at wetted layer l, computed by

$$f_l = K_l \cdot i_l = K_l \cdot \frac{\Delta h_l}{\Delta z} \tag{13}$$

Here, i_l is the hydraulic gradient of layer l; $\triangle h_l$ represents the change of hydraulic head within the lth layer. Combining Eqs. (12) and (13), we obtain:

$$\Delta h_l = \frac{f_l}{K_l} \cdot \Delta z \tag{14}$$

At the bottom of lth wetted layer, the hydraulic head h_l is obtained by summing the incremental heads Δh_l over all wetted computational layers $k \leq l$

$$h_l = h_0 - \sum_{k=1}^{l} \Delta h_k \tag{15}$$

in which h_0 is the boundary hydraulic head at the top of the wetted zone. Here, it is $h_0 = 0$ during the infiltration procedure, as the ponding depth is neglected (see Figure 3). Since the hydraulic head h_l consists of the pressure head ψ_l and the elevation z_l, the pressure head at the bottom of lth layer is evaluated as:

$$\psi_l = h_l - z_l \tag{16}$$

The pore water pressure can be computed as $u_l = \gamma_w \cdot \psi_l$, where γ_w is the unit weight of water. Each realization of the random variables **X** modeling the spatial variability of the hydraulic parameters of the soil results in different values of the saturated hydraulic conductivity and suction head at each soil layer. Based on these parameters values, the pore water pressure distribution within the wetted zone for each jth layer representing the wetting front can be computed.

2.5 Stability analysis of layered slope

The factor of safety associated with the wetting front having reached layer j is the minimum value among all the layers in the wetted zone:

$$FS_j(\mathbf{X}) = \min\{FS_{l,j}(\mathbf{X}), l = 1, \dots, j\} \tag{17}$$

where $FS_{l,j}$ is the factor of safety for a slip surface at the bottom of layer l and a wetting front at layer j, computed according to Eq. (1). Substituting $FS_{l,j}$ with Eq. (1), the complete expression is:

$$FS_j(\mathbf{X}) = \min\left\{\frac{(\gamma H_l \cos^2\beta - u_{l,j})\tan\varphi' + c'}{\gamma H_l \sin\beta\cos\beta}, l = 1, \dots, j\right\} \tag{18}$$

Eq. (18) computes the factor of safety associated with a wetting front at layer j, neglecting failures in slip surfaces below the wetting front. These failures are included by computing the factor of safety associated with a dry soil ($j = 0$), which is:

$$FS_0(\mathbf{X}) = \min\{FS_{l,0}(\mathbf{X}), l = 1, \dots, n\}$$

$$= \min\left\{\frac{\tan\varphi'}{\tan\beta} + \frac{c'}{\gamma H_l \sin\beta\cos\beta}, l = 1, \dots, n\right\} \quad (19)$$

The probability distribution of the factor of safety at each time step can be evaluated by Monte Carlo simulation through generating samples of the random vector **X** describing the random fields. For each realization of the random fields, the evolution of the factor of safety with time is computed by combining Eqs. (18), (19) and (11).

3. Reliability analysis

3.1 Failure condition

For the infinite slope model, slope failure occurs when the factor of safety is less than unity. During the infiltration procedure, when the wetting front reaches the bottom of layer j, the factor of safety $FS_j(\mathbf{X})$ is obtained by Eq. (17). Hence, the condition $FS_j(\mathbf{X}) < 1$ represents instantaneous failure when the wetting front reaches layer j and the corresponding probability of failure is $\Pr[FS_j(\mathbf{X}) < 1]$. Usually, one is interested in knowing the probability that failure has occurred at any wetting front location smaller or equal to j. That is, the probability that failure has occurred at any time prior to the time needed for the water to reach layer j. This probability of failure at any wetting front $k \leq j$ is termed cumulative failure probability and can be expressed as follows:

$$P_{f_j} = \Pr(F_j) = \Pr[\exists k \in \{0, \dots, j\}: FS_k(\mathbf{X}) < 1] \quad (20)$$

The failure condition of the above cumulative failure probability can be expressed by the following limit-state function:

$$g_j(\mathbf{X}) = \min\{FS_k(\mathbf{X}), k = 0, \dots, j\} - 1 \quad (21)$$

Here, $FS_k(\mathbf{X})$ is the factor of safety associated with wetting front k, which can be evaluated by application of Eqs. (18) and (19). Slope failure at any layer smaller or equal to j occurs for any realization $\mathbf{x}$ of $\mathbf{X}$ for which $g_j(\mathbf{x}) < 0$. Hence, the cumulative probability of failure P_{f_j} is given by:

$$P_{f_j} = \Pr[g_j(\mathbf{X}) < 0] \quad (22)$$

The probability in Eq. (22) is evaluated through application of Subset Simulation.

3.2 Subset Simulation

The continuous random fields modeling the spatial variability of the permeability parameters of the soil are represented by random variables corresponding to the midpoints of the discrete soil layers, as discussed in Section 2.2. If the random fields have small scale of fluctuation, a large number of random variables will be required in order to capture their point-to-point variability (see Li and Der Kiureghian 1993). Efficient estimation of the probability of Eq. (22) in such high dimensional problems can be achieved by application of Subset Simulation (Au and Beck 2001). Subset Simulation is an adaptive Monte Carlo method that estimates probabilities of rare events efficiently independent of the number of random variables. This is achieved by expressing the rare event as an intersection of more frequent events that are estimated by application of Markov chain Monte Carlo (MCMC) sampling (Papaioannou et al.

2015).

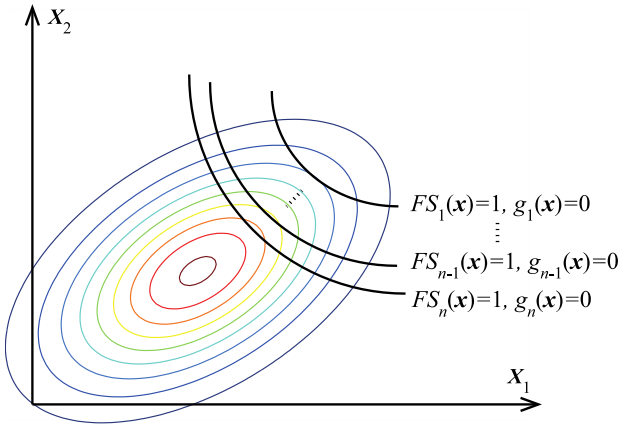

Figure 5. Failure domain corresponding to the computation step

Following Eq. (22), F_j denotes the failure at any wetting front $k \leq j$. It is easy to see that F_{j-1} implies F_j, i.e. the former is a subset of the latter: $F_{j-1} \subset F_j$. Hence, for the sequence of failure events $F_0, F_1, F_2, \dots, F_n$, where n is the number of layers, it holds $F_0 \subset F_1 \subset F_2 \subset \cdots \subset F_n$, see also Figure 5. In the following we assume that for the initial state of the infinite slope, the probability of failure is zero, $\Pr(F_0) = 0$; we can therefore omit the event F_0 in the following. Subset Simulation is applied to estimate the probability $\Pr(F_n)$. To this end, the event F_n is further decomposed into a sequence of nested intermediate failure events $F_{n1}, F_{n2}, \dots, F_{nM}$, with $F_{n1} \supset F_{n2} \supset \cdots \supset F_{nM}$, and $\Pr(F_n)$ is expressed as a product of conditional probabilities:

$$P_{f_n} = \Pr(F_n) = \Pr(\cap_{i=1}^{M} F_{ni}) = \Pr(F_{n1}) \prod_{i=2}^{M} \Pr\left(F_{ni} | F_{n(i-1)}\right) \qquad (23)$$

The intermediate events are defined as $F_{ni} = [g_n(\mathbf{x}) < b_{ni}]$, where $b_{n1} > b_{n2} > \cdots > b_{nM} = 0$. The values of b_{ni} are chosen adaptively such that the estimates of the conditional probabilities correspond to a chosen value p_0. This is achieved by simulating samples of $\mathbf{X}$ conditional on each intermediate failure event $F_{n(i-1)}$. For each sample, the limit-state function $g_n(\mathbf{x})$ is evaluated and the samples are ordered in

increasing order of magnitude of the limit-state function values. The threshold b_{ni} is set to the p_0-percentile of the ordered samples. The procedure is repeated until the maximum level M is reached, for which $b_{nM} = 0$. To estimate b_{n1}, unconditional samples of $\mathbf{X}$ are obtained by crude Monte Carlo. Samples of $\mathbf{X}$ conditional on the events $F_{ni}, i = 1, \dots, M-1$, are computed by MCMC sampling using as seeds the samples conditional on $F_{n(i-1)}$ for which $g_n(\mathbf{x}) < b_{ni}$. The probability $\Pr(F_n)$ is the obtained as:

$$\Pr(F_n) = p_0^{M-1} \hat{P}_{nM} \tag{24}$$

where $\hat{P}_{nM}$ is the estimate of $\Pr\left(F_{nM} | F_{n(M-1)}\right)$ and is given by the ratio of the number of samples for which $g_n(\mathbf{x}) < 0$ over the total number of samples simulated conditional on $F_{n(M-1)}$. At the final level of Subset Simulation for estimating F_n, the available samples conditional on $F_{nM} = F_n$ are used to start a new Subset Simulation run for estimating the conditional probability $\Pr(F_{n-1}|F_n)$. That is, samples conditional on the failure domain $F_{n-1} \subset F_n$ are obtained by sampling $\mathbf{X}$ conditional on a sequence of intermediate failure domains through MCMC and the probability $\Pr(F_{n-1}|F_n)$ is estimated in a manner analogous to Eq. (24). The probability $\Pr(F_{n-1})$ is then obtained as:

$$\Pr(F_{n-1}) = \Pr(F_n) \Pr(F_{n-1}|F_n) \tag{25}$$

This procedure is repeated for estimation of the remaining probabilities $\Pr\left(F_j\right), j = 1, \dots, n-2$. An efficient algorithm for estimating the conditional probabilities $\Pr(F_{n-1}|F_n)$ is provided in (Papaioannou et al. 2015).

4. Numerical example

We consider an infinite slope in sandy soil subject to an intense rainfall event. The soil column is 5 m deep above bedrock. The slope angle and effective friction angle are $\beta = 18°$ and $\varphi' = 30°$, respectively, while the effective cohesion is assumed zero, i.e. $c' = 0$ and the unit weight of sand is 20kN/m^3. The saturated vertical hydraulic conductivity K and suction head S are modeled as homogeneous lognormal random fields with medians 2.99 cm/h and 6.13 cm, respectively. These values are typical values for loamy sands (Rawls et al. 1983). We assume that the point-wise cross-correlation coefficient between K and S is $\rho_c = -0.5$. In a parametric study, we vary the standard deviation and the scale of fluctuation of the decimal logarithms of the two random fields. The random fields are discretized into 100 layers. The parameters of the Green and Ampt model for loamy sand are taken from Rawls et al. (1982) as given in Table 1.

Table 1. Parameters for Green and Ampt model

Variable	η	θ_0
Value	0.437	0.125

4.1 Wetting front development

First, we investigate the influence of the scale of fluctuation and standard deviation of the two random fields on the wetting front development. Figure 6 presents the development of the mean depth of the wetting front with time evaluated with 5000 samples (realizations) of the random fields. The time period of interest is 120 hours (5 days) after the start of the rainfall event.

Figure $6(a)$ compares the wetting front development for different values of the scale of fluctuation of the two random fields. The standard deviation of the decimal

logarithms for both fields $\sigma_{\log_{10}(K,S)}$ is here 0.5. It is shown that in the case of a smaller scale of fluctuation, the water infiltrates slower towards the bottom of the soil column. This can be explained by the fact that a small scale of fluctuation implies a larger variability within the wetted zone and hence more frequent occurrence of lower values of K. The flow within the wetted zone is dictated by the low values of K, as evident from the use of the harmonic mean of the saturated hydraulic conductivity in Eq. (7). For a rainfall period of more than 80 hours, the infiltration rates of the larger scale of fluctuation cases ($r \geq 0.5$m) are nearly identical. It can be inferred that, with the wetting front advances, the difference of the effective hydraulic conductivity K_{eff} within wetted zone in those cases become smaller. In the limit case $r = \infty$, the hydraulic conductivity is constant in space and hence modeled by a single random variable.

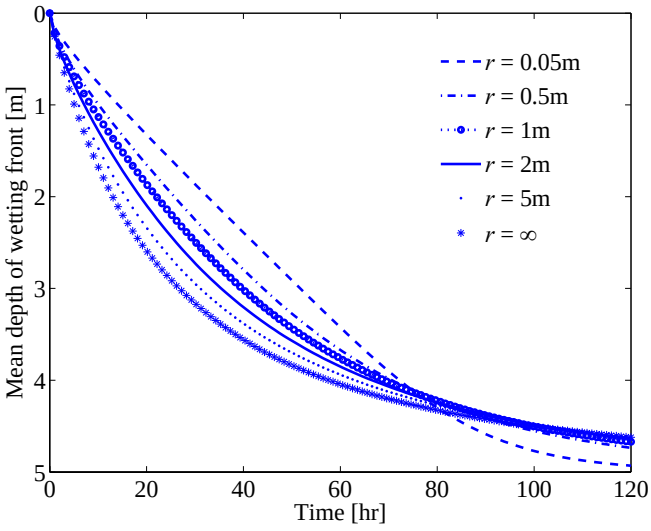

(a) Influence of the scale of fluctuation r for a constant $\sigma_{\log_{10}(K,S)} = 0.5$

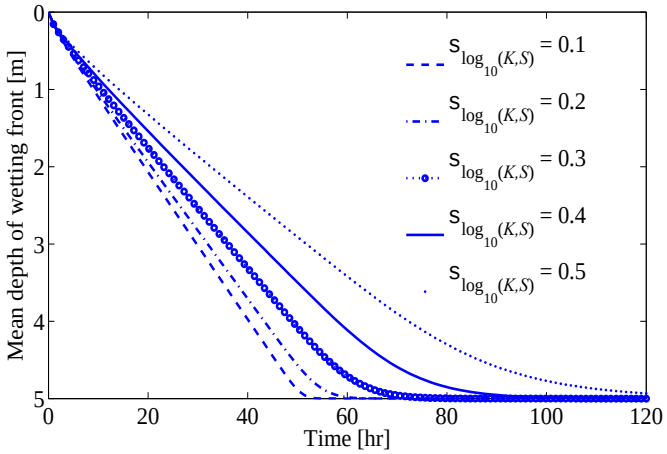

(b) Influence of the standard deviation $\sigma_{\log_{10}(K,S)}$ for a constant $r = 0.05m$

Figure 6. The mean wetting front development

Figure $6(b)$ demonstrates the influence of $\sigma_{\log_{10}(K,S)}$ of the two random fields. Here, the scale of fluctuation is fixed at $0.05m$. As $\sigma_{\log_{10}(K,S)}$ increases, the wetting front moves slower towards the bottom of the soil column. This is due to the fact that a large standard deviation increases the average occurrence of low values of the hydraulic conductivity and hence decreases its harmonic mean within the wetted zone.

4.2 Pore-pressure building up

Throughout the infiltration process, the variable permeability within the sandy soil will influence the pore water pressure buildup and further influence the factor of safety of the infinite slope. Figure 7 shows the pore water pressure distribution for the two realizations of the hydraulic conductivity shown in Figure 2, corresponding to scales of fluctuation of $0.05m$ and $5m$, respectively, and for two different depths of the wetting front, namely $2.5m$ and $5m$. The suction head is kept constant and equal to its median 6.13 cm. In the case with smaller scale of fluctuation ($r = 0.05m$), the spatial variability of the hydraulic conductivity within the wetted zone introduces large local hydraulic gradients, which lead to faster changes in the pore water pressure. This can be

clearly observed in Figure 7, where for a small scale of fluctuation ($r = 0.05\text{m}$) the pore water pressure presents larger spatial variation along the depth of the soil column, whereas for a larger scale of fluctuation ($r = 5\text{m}$), the distribution of pore water pressure represented by the dash-dot line is smoother. The pore water pressure build-up at the areas with steep gradient of the hydraulic conductivity is evident when comparing Figures 2 and 7. Moreover, the large hydraulic gradients in the highly fluctuating case introduce positive pore water pressure at shallow depths of the wetting front, see Figure 7(a). Based on Eq. (1), the factor of safety decreases as the pore water pressure increases and as the depth of the potential slip surface decreases. Hence, positive pore water pressure at a shallow depth of the wetting front will undermine the stability of the slope and favor shallow slope failure.

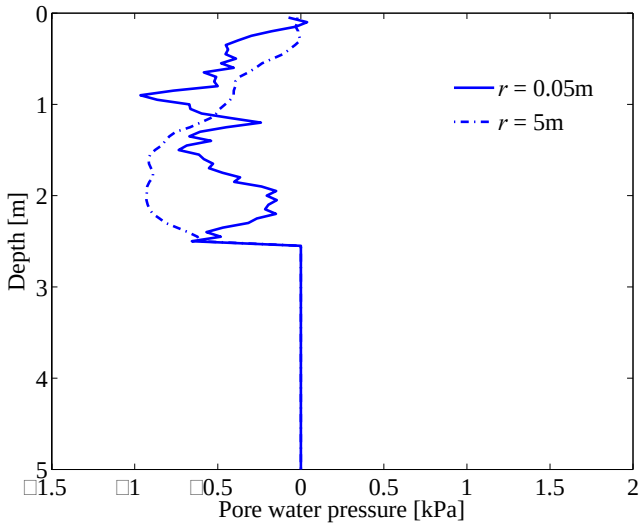

(a) Depth of wetting front = 2.5m

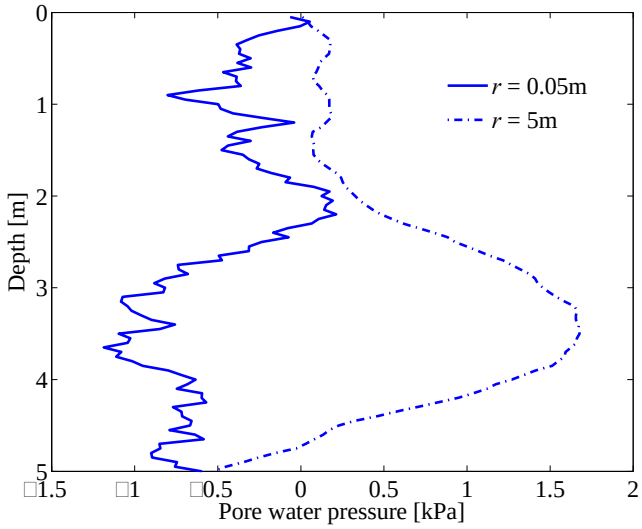

(b) Depth of wetting front = 5m

Figure 7. Pore water pressure distributions for the realizations of the hydraulic conductivity of **Fig. 2**.

4.3 Mean factor of safety

The mean factor of safety is obtained by generating random realizations of the random fields representing the hydraulic conductivity and suction head and taking the mean value of the factor of safety, according to Eq. (17). We vary $\sigma_{\log_{10}(K,S)}$ and r to assess their influences on the mean factor of safety. The mean factor of safety is evaluated with 5000 Monte Carlo samples.

Figure $8(a)$ shows the influence of the scale of fluctuation on the mean factor of safety with respect to the wetting front development, for $\sigma_{\log_{10}(K,S)}$ fixed at 0.5. Since the pore water pressure increases due to the wetting front development, the mean factor of safety decreases during the infiltration procedure in all cases. The transient behavior of the mean factor of safety is characterized by a fast reduction right after the beginning of the rainfall event, followed by a slower decrease as the wetting front moves closer towards the bedrock. The reduction is larger in the case where the scale of fluctuation is smaller and hence the spatial variability of the permeability parameters is higher. This is

because high spatial variability of the hydraulic conductivity within the wetted zone introduces large hydraulic gradients as also illustrated in Figure 7 and therefore increases the likelihood of high pore water pressure at shallow depths of the wetting front, which are critical for the stability of the slope. Hence the factor of safety reaches its minimum on average at a smaller depth of the wetting front in highly fluctuating soils as compared to more homogeneous soils. Moreover, due to the low pressure gradients, the minimum factor of safety in soils with larger scale of fluctuation is larger than the one in highly fluctuating soils.

Figure $8(b)$ depicts the influence of $\sigma_{\log_{10}(K,S)}$ on the mean factor of safety of the slope. Here, the scale of fluctuation is fixed at $r = 0.05\text{m}$. The resulting mean factor of safety has a similar transient behavior in all cases. Its value decreases in the first 1m and asymptotically approaches a minimum value. This minimum value decreases with increase of $\sigma_{\log_{10}(K,S)}$. This is because as the standard deviation increases, the likelihood of high positive pressure at shallow depths becomes higher.

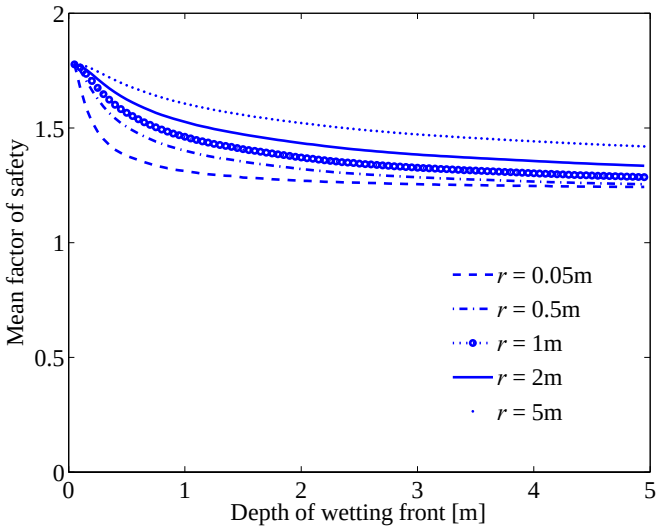

(a) Influence of the scale of fluctuation r for a constant $\sigma_{\log_{10}(K,S)} = 0.5$

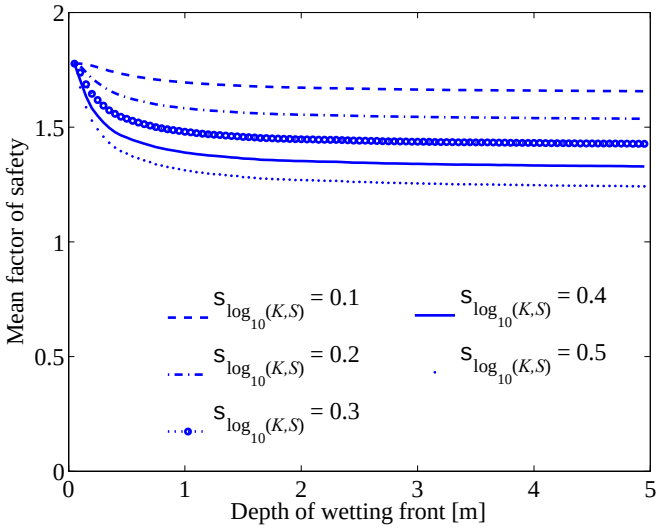

(b) Influence of the standard deviation $\sigma_{\log_{10}(K,S)}$ for a constant $r = 0.05\text{m}$

Figure 8. Mean factor of safety in terms of wetting front development.

Next we investigate the change of the critical slip surface within the wetted zone with respect to the development of the wetting front. The factor of safety of each potential slip plane within the dry zone remains constant during the rainwater infiltration and equals $tan\varphi' / tan\beta$, because positive pore water pressure only exists in the wetted zone and pore water pressure is negative in the dry zone due to suction, see Eq. (1). Here, the critical slip surface corresponds to the plane with minimum factor of safety in the wetted zone of the soil column. Figure $9(a)$ shows the influence of the scale of fluctuation on the mean depth of critical slip surface within the wetted zone with wetting front development for $\sigma_{\log_{10}(K,S)} = 0.5$. It is shown that the mean depth of the critical slip surface approaches the ground surface as the scale of fluctuation decreases. Hence small scales of fluctuation r favor shallow slope failure. This agrees with Figure $8(a)$, where it was shown that for small r the factor of safety on average reduces faster to its minimum value with the wetting front development. Conversely, for larger scales of fluctuation the critical slip surface increases linearly with the wetting

front development and therefore the mean factor of safety decreases slower. In Figure $9(b)$, we fix the scale of fluctuation at $r = 0.05m$ and study the influence of the standard deviation $\sigma_{\log_{10}(K,S)}$ on the mean depth of critical slip surface. For higher values of $\sigma_{\log_{10}(K,S)}$, the critical slip surface moves closer to the ground surface. However, the influence of $\sigma_{\log_{10}(K,S)}$ is less pronounced than the influence of the scale of fluctuation. This agrees with the result of Figure $8(b)$, which shows that changes in $\sigma_{\log_{10}(K,S)}$ will not significantly influence the transient behavior of the mean factor of safety. It only affects the minimum value of the mean factor of safety.

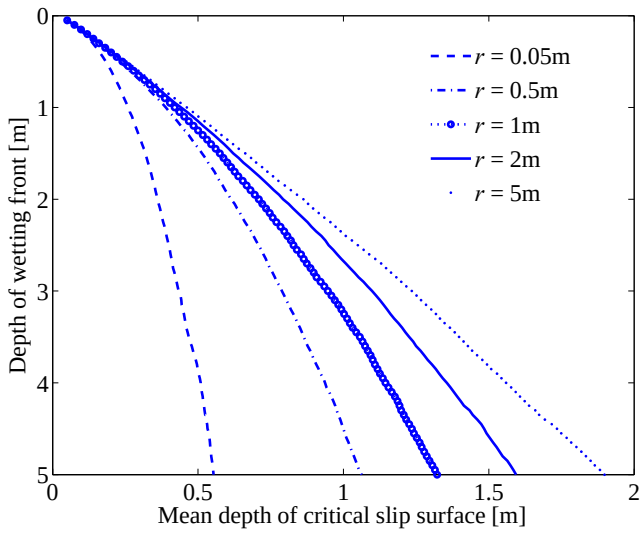

(a) Influence of the scale of fluctuation r for a constant $\sigma_{\log_{10}(K,S)} = 0.5$

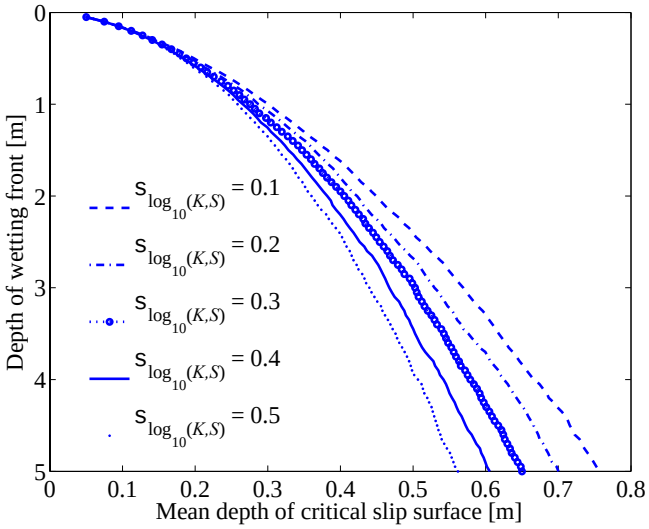

(b) Influence of the standard deviation $\sigma_{\log_{10}(K,S)}$ for a constant $r = 0.05$m

Figure 9. Critical slip surface distribution within wetted zone

4.4 Probability of failure

In most cases, the probability of failure of the infinite slope due to infiltration is small. We therefore employ Subset Simulation for computing it (see Section 3.2). 1000 samples are used for estimating each intermediate conditional probability.

Figure $10(a)$ shows the influence of the scale of fluctuation on the probability of failure in function of the wetting front development, for a fixed $\sigma_{\log_{10}(K,S)} = 0.5$. As the wetting front depth increases, the probability of failure approaches the same value for all scales for fluctuation. However, this value is reached much faster for smaller scales of fluctuation, i.e. for larger variability of the permeability within the soil layer. This agrees with Figure $8(a)$ where it is shown that in cases with smaller scales of fluctuation the factor of safety decreases faster at shallower depths of the wetting front. It can be concluded that in soils with high spatial variability the probability of failure of the infinite slope is higher at the start of the rainfall event compared to soils with low variability.

Figure $10(b)$ illustrates the influence of $\sigma_{\log_{10}(K,S)}$ on the probability of failure of the infinite slope for a fixed (small) scale of fluctuation $r = 0.05\text{m}$. We see that in all cases the probability of failure increases fast to a constant value within $0{\sim}1\text{m}$ wetted depth. This is because the scale of fluctuation is small and hence failure is more likely to occur at shallow depths. Also, as illustrated in Figure $9(b)$, the standard deviation in log scale does not have significant influence on the mean position of the critical slip surface within the wetted zone. The logarithm of the probability of failure in the case with different $\sigma_{\log_{10}(K,S)}$ converges to different values as the wetting front advances. These values increase exponentially with increase of $\sigma_{\log_{10}(K,S)}$, which indicates that $\sigma_{\log_{10}(K,S)}$ has significant influence on the reliability of the infinite slope. Moreover, it is shown that as the standard deviation increases the probability of failure increases faster with the wetting front development. This is because, although $\sigma_{\log_{10}(K,S)}$ does not influence the mean depth of the critical slip surface, it has an impact on the variance.

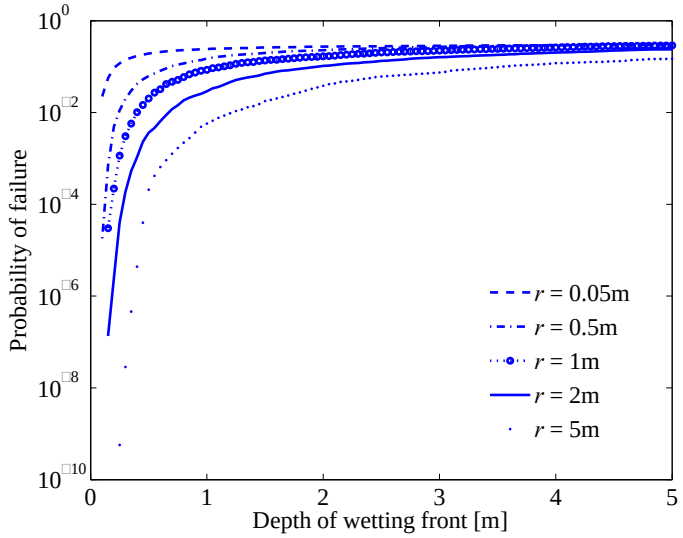

(a) Influence of the scale of fluctuation r for a constant $\sigma_{\log_{10}(K,S)} = 0.5$

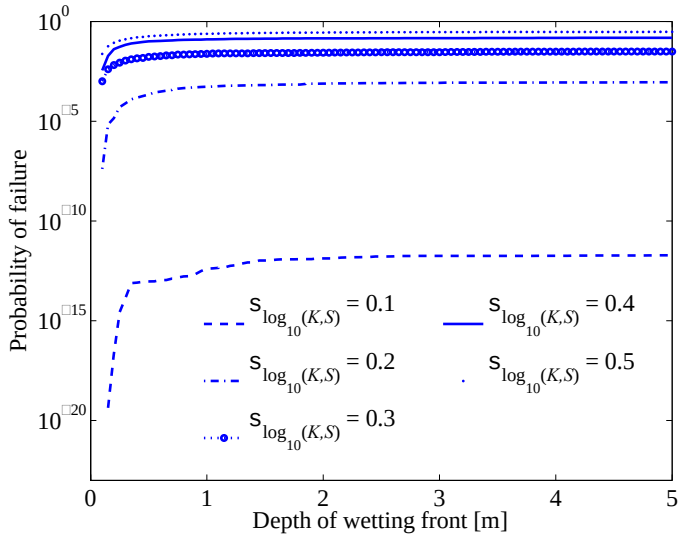

(b) Influence of the standard deviation $\sigma_{\log_{10}(K,S)}$ for a constant $r = 0.05$m

Figure 10. Decimal logarithm of the probability of failure in terms of wetting front development.

6. Concluding remarks

This paper presented a probabilistic stability analysis of an infinite slope subjected to non-stop intense rainfall event. The physical-based infiltration model is a multi-layered extension of the Green and Ampt model and assumes a distinct wetting front between wetted and dry zones. The spatial variability of saturated hydraulic conductivity and suction head is modeled through correlated random fields. The mean behavior of the wetting front development and the factor of safety of the slope were evaluated with Monte Carlo simulation and the cumulative probability of failure was computed with Subset Simulation. The Green and Ampt model assumes that a well defined wetting front separates the wetted and dry zone during the rainwater infiltration. This approximation is good for sandy soil, in which the rainwater is driven by gravity with uniform water content (Bear 1972). For other soils, such as clayey soil, the water flow will not move like a piston and the shape of wetting front is not as sharp as in sandy soil.

Through a case study, we investigated the influence of the scale of fluctuation r and the standard deviation of the logarithm of the hydraulic conductivity and the suction head $\sigma_{\log_{10}(K,S)}$ on the wetting front development, the mean factor of safety and the probability of failure of the slope. Decreasing r or increasing $\sigma_{\log_{10}(K,S)}$ will increase the variability of the soil layer permeability. This increases the likelihood of occurrence of low permeability values, which decreases effective hydraulic conductivity K_{eff} within the wetting zone, thus leading to slower movement of the wetting front. A decrease in the scale of fluctuation r has a significant influence on the transient behavior of the factor of safety. It was shown that by decreasing r, the mean factor of safety decreases faster with the wetting front development, due to larger pore pressure build-up at shallow depths, which favors shallow slope failure. This leads to large failure probabilities at shallow depths of the wetting front. A change in $\sigma_{\log_{10}(K,S)}$ does not have significant influence on the mean depth of the critical slip surface within the wetted zone. Therefore, the factor of safety drops to a lower value at similar depth of wetting front regardless of $\sigma_{\log_{10}(K,S)}$. This lower value decreases with increase of $\sigma_{\log_{10}(K,S)}$. The probability of failure increases faster with the development of the wetting front at the beginning of the infiltration with increasing $\sigma_{\log_{10}(K,S)}$, while the impact of $\sigma_{\log_{10}(K,S)}$ on the maximum value of the probability of failure is shown to be significant.

References:

Au, S. K., and J. L. Beck. 2001. "Estimation of Small Failure Probabilities in High Dimensions by Subset Simulation." *Probabilistic Engineering Mechanics* 16: 263-277.

Bauters, T. W. J., D. A. DiCarlo, T. S. Steenhuis and J. Y. Parlange. 2000. "Soil Water Content Dependent Wetting Front Characteristics in Sands." *Journal of Hydrology* 231-232: 244-254.

Bear, J. 1972. *Dynamics of Fluids in Porous Media*. Mineola, New York: Dover.

Chen, L., and M. H. Young. 2006. "Green-Ampt Infiltration Model for Sloping Surface." *Water resources research* 42(7): W07420.

Chu, X. F., and M. A. Marino. 2005. "Determination of Ponding Condition and Infiltration into Layered Soils under Unsteady Rainfall." *Journal of Hydrology* 313: 195-207.

Corominas, J., J. Moya, and M. Hürlimann. 2002. "Landslide Rainfall Triggers in the Spanish Eastern Pyrenees." *Proc. 4th EGS Plinius Conference*. Mallorca, October 2-4.

Der Kiureghian, A., and J. B. Ke. 1988. "The Stochastic Finite Element Method in Structural Reliability." *Probabilistic Engineering Mechanics* 3(2): 83-91.

Freeze, R. A. and J. A. Cherry. 1979. *Groundwater*. Upper Saddle River, New Jersey: Prentice Hall.

Gelhar, L. W. 1986. "Stochastic Subsurface Hydrology from Theory to Application." *Water Resources Research* 22(9): 135-145.

Green, W. H. and G. A. Ampt. 1911. "Studies on Soil Physics, Part I – the Flow Air and Water through Soils." *Journal of Agricultural Science* 4(1): 1-24.

Griffiths, D. V., J. Huang, and G. A. Fenton. 2011. "Probabilistic Infinite Slope Analysis." *Computers and Geotechnics* 38(4): 577-584.

Horn, R., and C. Johnson. 1985. *Matrix Analysis*. New York: Cambridge University Press.

Li, C. C., and A. Der Kiureghian. 1993. "Optimal Discretization of Random Fields." *Journal of Engineering Mechanics* 119(6): 1136-1154.

Liu, J. T., J. B. Zhang, and J. Feng. 2008. "Green–Ampt Model for Layered Soils with Nonuniform Initial Water Content Under Unsteady Infiltration." *Soil Science Society of America Journal* 72(4): 1041-1047.

Muntohar, A. S. and H. Liao. 2010. "Rainfall Infiltration: Infinite Slope Model for Landslides Triggering by Rainstorm." *Natural Hazards* 54(3): 967–984.

Papaioannou, I., W. Betz, K. Zwirglmaier, and D. Straub. 2015. "MCMC Algorithms for Subset Simulation." http://www.era.bgu.tum.de/fileadmin/w00bkd/www/Papers/MCMC_SubS_Sept14.pdf.

Phoon, K. K., and F. H. Kulhawy. 1999. “Characterization of Geotechnical Variability.” *Canadian Geotechnical Journal* 36 (4): 612-624.

Polemio, M. 1997. “Rainfall and Senerchia Landslides, Southern Italy.” *Proc. 2nd Pan-American Symposium on Landslides, 2nd COBRAE, Rio de Janeiro*, November, 10-14.

Polemio, M., O. Petrucci, O. Petrucci, and C. Irpi. 2000. “Rainfall as a landslide triggering factor: an overview of recent international research.” *Landslides in Research Theory and Practice, Proceedings of the 8th International Symposium on Landslides*, Cardiff, June, 26-30.

Rawls, W. J., D. L. Brakensiek, and K. E. Saxton. 1982. “Estimation of Soil Water Properties.” *Transactions of the American Society of Agricultural Engineers* 25(5): 1316-1320 &1328.

Rawls, W., D. Brakensiek, and N. Miller. 1983. “Green-Ampt Infiltration Parameters from Soils Data.” *Journal of Hydraulic Engineering* 109(1): 62–70.

Rubinstein, R. Y., and D. P. Kroese. 2008. *Simulation and the Monte Carlo method*. Hoboken: N. J. Wiley.

Santoso, A. M., K. Phoon, and S. Quek. 2011. “Effect of 1D Infiltration Assumption on Stability of Spatially Variable Slope.” *Geo-Risk 2011:* 704-711.

Takara, A. K., and Y. Yamashiki. 2011. “Enhanced Assessment of Rainfall and Hydrologic Effects on the Triggering Mechanism of Shallow Landslides.” *Annuals of Disaster Prevention Research Insitute*, Kyoto University, 54B: 83-93.

Vanmarcke, E. H. 1983. *Random Fields: Analysis and Synthesis*. Cambridge: MIT Press.

Wu, T. H., and M. A. Abdel-Latif. 2000. “Prediction and Mapping of Landslide Hazard.” *Canadian Geotechnical Journal* 37(4): 579–90.

Yeh, H. F., C. C. Lee, and C. H. Lee. 2008. “A Rainfall-infiltration Model for Unsaturated Soil Slope Stability.” *Journal of Environmental Engineering and Landscape Management* 18(4): 261-268.

Zêzere, J. L., R. M. Trigo, and M. Fragoso, S. C. Oliveira, and R. A. C. Garcia. 2008. “Rainfall-triggered Landslides in the Lisbon Region over 2006 and Relationships with the North Atlantic Oscillation.” *Natural Hazards and Earth System Science* 8(3): 483–499.

Zhang, L. L., L. M. Zhang, and W.H. Tang. 2005. “Rainfall-induced Slope Failure Considering Variability of Soil Properties.” *Géotechnique* 55(2): 183-188.